Non-Conventional Discretization Grid Based FDTD for EM Wave Propagation in Magnetized Plasma Metallic Photonic Crystal

Mayank K. Chaudhari[1, 2, *]

Abstract—Photonic band gaps of plasma metallic photonic crystals can be tuned dynamically by subjecting it to external magnetic field leading to variety of applications. Dispersion characteristics of 2D photonic crystals are often studied by Finite Difference Time Domain (FDTD) method based on standard Yee's grid discretization schema, in which x- and y-components of fields are defined on different edges of the Yee's cell. However, finite difference equations for electromagnetic wave propagation in magnetized plasma involve interdependence of polarization currents and electric field in a manner that requires both x- and y-components of fields to be evaluated at the same spatial location. A non-conventional discretization technique is presented in which x- and y-components of fields are evaluated at the same spatial location. In this paper analysis of magnetized plasma metallic photonic crystals (PMPC) is presented using the new grid. However, the proposed discretization scheme can be used to introduce magnetized plasmas in any type of structures that can be studied on the basis of standard Yee's grid. For example, topics such as photonic band gap (PBG) cavities based on PMPC, PBG waveguides involving plasma, metamaterials, etc. can be very effectively studied using the approach presented in this paper. Interesting results are found when PMPC is subject to external magnetic field. Several new bands including two dispersion-less flat bands appear and the existing bands with an exception of first band slightly shift upward when PMPC is subjected to an external transverse magnetic field. The location of flat bands and the location and width of forbidden band gaps can be controlled by external magnetic field as well as plasma parameters. New band gaps appearing for lower r/a for magnetized PMPC can be utilized for several applications such as PBG cavity design for gyrotron devices.

1. INTRODUCTION

The concept of photonic crystals (PCs) has gained increasing popularity since original proposition by Yablonovitch and John in 1987 owing to their incredible capacity to mould the flow of light and their tunefulness [1, 2]. Properties of PCs are dramatically controlled by their structural parameters and offer vast variety of applications such as brag-reflectors, filters, anti-reflecting coatings, fibers, cavities for devices such as lasers and gyrotron, Nano-cavities for enhancement of light-matter interaction, cloaking, self-focusing media, sensors, ultra-fast photonic circuits etc. [3–9]. These are structures having periodicity in one, two, or three dimensions with unit cell dimensions of the order of wavelength of light. PCs appear in nature in the form of structural coloration. The colors in the peacock's feather and the wings of Morpho butterflies as well as many opals are samples of superior natural architecture [10–12]. These colors are exhibited because of interference of light reflected and transmitted by these nano-structures.

The concept of PCs is extended to metallic photonic crystals (MPC) and plasma metallic photonic crystals (PMPCs). Using metal inclusions provides higher power handling capability and introducing plasma adds additional degree of freedom for tuning photonic band gaps [13–15]. Band structures of plasma-dielectric and plasma-metallic photonic crystals can be engineered by altering plasma parameters. Moreover, dynamical tunefulness of PMPC by external magnetic field opens avenues for new applications [13, 16]. PCs, MPCs, and PMPCs are extensively studied in recent decades. All of these have been analyzed by techniques such as plane wave expansion method, transfer matrix method, multiple multipole method, finite element method, Finite Difference Time Domain (FDTD), etc. [17]. The need is felt for FDTD implementation based on nonconventional discretization grid as opposed to conventional electromagnetic problems, in formalism of magnetized PMPC x- and y-components of electric fields are interdependent in such a way that they must be evaluated at same spatial location. In standard Yee's grid, x- and y-components of electric field are defined along different edges of the unit cell of the grid. This interdependence is via polarization currents in plasma. Thus, to solve this problem a modified discretization grid structure is introduced. Simulations based on new grid are in excellent agreement with simulations based on standard Yee's grid and other techniques. In this paper modified discretization grid is used to analyze magnetized PMPC. Study of PMPC and magnetized PMPC in triangular lattice arrangements is also presented which is not reported till now. The approach presented herein can be used for introducing magnetized plasmas in any FDTD simulation.

2. THEORETICAL MODEL FOR PMPC

2D PMPC can be realized by placing metallic rods in plasma background. Fig. 1 shows cross-sectional view of PMPCs along with reciprocal lattices in square as well as triangular lattice arrangements. Dispersion characteristics of these PCs are obtained by analyzing the response of the structure along the boundaries of irreducible Brillion zone. For FDTD analysis a primitive unit cell is chosen to span the computational domain which is terminated by periodic boundary condition. Unit cells considered in present analysis are shown by square and rectangle for square and triangular lattice respectively. To avoid non-orthogonal FDTD, a modified primitive unit cell originally proposed by Umenyi et al. is used to span the computational domain for triangular lattice [18].

Electromagnetic wave propagation in plasma medium can be described in terms of polarization
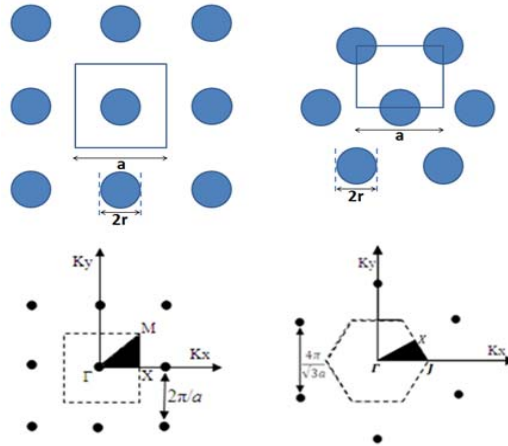
Figure 1. Cross sectional view of PMPC in configuration space along with reciprocal lattices. Dark circles represent metallic rods placed in background of plasma. Square and rectangle shown in square and triangular lattice respectively in configuration space show the primitive unit cells considered to span the computational domain. Irreducible Brillion zones are shown by shaded region in respective reciprocal lattices.

currents [13, 15]. Maxwell's equations in plasma medium may be written as follows

$$\frac{\partial \mathbf{H}}{\partial t} = -\frac{1}{\mu_0} \nabla \times \mathbf{E} \tag{1}$$

$$\frac{\partial \mathbf{E}}{\partial t} = \frac{1}{\varepsilon_0} \left(\nabla \times \mathbf{H} - \mathbf{J} \right) \tag{2}$$

where $\mathbf{J} = J_x \hat{i} + J_y \hat{j} + J_z \hat{k}$ is the polarization current density vector which includes the information of frequency dependent permittivity of plasma; $\mathbf{E} = E_x \hat{i} + E_y \hat{j} + E_z \hat{k}$ is the electric field strength vector; $\mathbf{H} = H_x \hat{i} + H_y \hat{j} + H_z \hat{k}$ is the magnetic field strength; ε_0 and μ_0 are permittivity and permeability of free space. The time varying polarization current density may be expressed by [find reference — EM wave in magnetized plasma]

$$\frac{d\mathbf{J}}{dt} + \upsilon \mathbf{J} = \varepsilon_0 \omega_p^2 \mathbf{E} + \omega_c \times \mathbf{J} \tag{3}$$

where $\omega_c = \omega_{cx} \hat{i} + \omega_{cy} \hat{j} + \omega_{cz} \hat{k} = (e\mathbf{B}/m)$ is the electron cyclotron frequency, ω_p the angular plasma oscillation frequency and υ the plasma collision frequency. For transverse magnetic field $\omega_c = \omega_{cz} \hat{k} = (eB/m)\hat{k}$, where, $\mathbf{B}$ is the applied magnetic field, e the electronic charge and m the mass of electron. Since x- and y-components of electron cyclotron frequency are zero, external magnetic field does not influence plasma polarization current along z-direction. Hence, only TE mode is influenced by transverse magnetic field applied to the PMPC. x- and y-components of polarization current are as follows

$$\frac{dJ_x}{dt} + \upsilon J_x = \varepsilon_0 \omega_p^2 E_x - \omega_{cz} J_y \tag{4}$$

$$\frac{dJ_y}{dt} + \upsilon J_y = \varepsilon_0 \omega_p^2 E_y + \omega_{cz} J_x \tag{5}$$

Using Eq. (4) and Eq. (5) updating equations compatible with FDTD implementations for plasma polarization currents may be written as follows

$$J_x^{n+1/2} = \frac{4s_1 s_2 - \omega_{cz}^2}{4s_1^2 + \omega_{cz}^2} J_x^{n-1/2} + \frac{4s_1 \varepsilon_0 \omega_p^2}{4s_1^2 + \omega_{cz}^2} E_x^n - \frac{2\omega_{cz}(s_1 + s_2)}{4s_1^2 + \omega_{cz}^2} J_y^{n-1/2} - \frac{2\varepsilon_0 \omega_{cz} \omega_p^2}{4s_1^2 + \omega_{cz}^2} E_y^n \tag{6}$$

$$J_y^{n+1/2} = \frac{4s_1 s_2 - \omega_{cz}^2}{4s_1^2 + \omega_{cz}^2} J_y^{n-1/2} + \frac{4s_1 \varepsilon_0 \omega_p^2}{4s_1^2 + \omega_{cz}^2} E_y^n + \frac{2\omega_{cz}(s_1 + s_2)}{4s_1^2 + \omega_{cz}^2} J_x^{n-1/2} + \frac{2\varepsilon_0 \omega_{cz} \omega_p^2}{4s_1^2 + \omega_{cz}^2} E_x^n \tag{7}$$

where $s_1 = \frac{1}{dt} + \frac{\upsilon}{2}$ and $s_2 = \frac{1}{dt} - \frac{\upsilon}{2}$. As obviously seen from difference equations for J_x and J_y, the x- and y-components of electric field and polarization currents are interdependent in such a manner that they must be computed at the same spatial location. Spatial indices are deliberately dropped from Eq. (6) and Eq. (7) as all the quantities involved are computed at the same spatial position, i.e., corresponding to same spatial location. The superscripts denote time step in accordance with standard FDTD convention.

3. SIMULATION METHOD BASED ON MODIFIED DISCRETIZATION GRID

FDTD method is based on the principle of solving finite difference equations corresponding to Maxwell's laws of electromagnetics at every spatial node and time step. At a particular instance in simulation, electric and magnetic fields at every spatial node are known for past time step and the fields for future time step are computed by solving Maxwell's equations in differential form [19, 20]. Simulations involving plasma medium require additional equations for updating plasma currents (Eq. (6) and Eq. (7)). Fig. 2 shows modified grid for TE polarization. Arrows represent x- and y-components of electric field and polarization currents density and the dots represent z-component of magnetic field. For TM polarization one need only interchange the interpretation of dots and arrows. The modified grid is essentially a superposition of two Yee's discretization grids shifted by half spatial step in both x- and y-direction. Thus all the formalism developed based on standard Yee's grid may very easily be implemented using new grid. In addition, the new grid must also follow stability and accuracy criteria derived originally
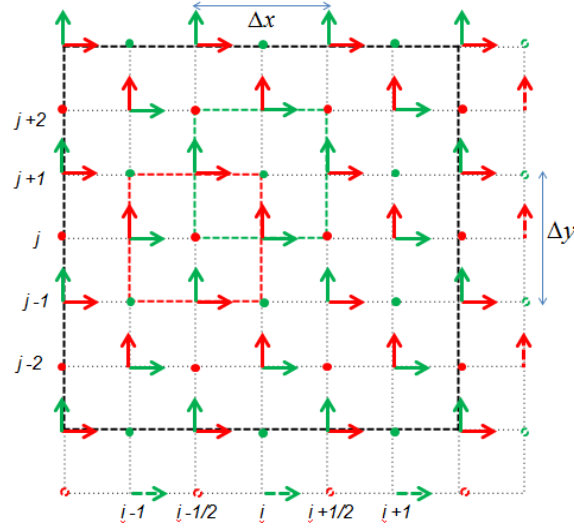
Figure 2. Modified discretization grid for magnetized plasmas. It is essentially superposition of two Yee's grid shifted by half spatial step. For TE polarization, the arrows represent x- and y-components of electric field and polarization current density and the dots represent z-component of magnetic field. Δx and Δy are spatial steps along x- and y-directions respectively. For FDTD implementation based on new grid, the grid points are indexed in multiples of integers along y-direction and in multiples of half-integers along x-direction. i and j are essentially the indices of the array elements of the arrays used to store the respective quantities at spatial steps. The computation domain is spanned by $(2n+1)\times(2m+1)$ node points. One row at bottom and one column on the right of node points is defined deliberately for terminating the grid with appropriate boundary condition.

for the standard Yee's grid such as Courant-Friedrichs-Lewy (CFL) criterion [17, 21]. This grid may very easily be extrapolated to 3 dimensions as well.

Henceforth, we may denote quantities whose x- and y-components are taken by ξ_{xy} and the quantities whose z-component is taken by η_z with the understanding that x- and y-components of electric field and polarization current and z-component of magnetic field are considered for TE polarization, and the x- and y-components of magnetic field and z-component of electric field and polarization current are considered for TM polarization. At even rows η_z is defined at integral steps and ξ_{xy} defined at half-integer steps whereas for odd rows it is vice-versa. Time steps are discretised in accordance with CFL criterion.

$$\Delta t \leq \Delta t_{\max} = \frac{1}{c\sqrt{1/\Delta x^2 + 1/\Delta y^2}} \tag{8}$$

The indexed quantities may be represented as follows

$$\left.\begin{aligned} \xi_{xy}^n(i,j) &= \xi_{xy}\left(\left(i+\frac{1}{2}\right)\Delta x, j\frac{\Delta y}{2}, n\Delta t\right) \\ \eta_z^n(i,j) &= \eta_z\left(i\Delta x, j\frac{\Delta y}{2}, n\Delta t\right) \end{aligned}\right\} \text{ for even rows}$$

$$\left.\begin{aligned} \xi_{xy}^n(i,j) &= \xi_{xy}\left(i\Delta x, j\frac{\Delta y}{2}, n\Delta t\right) \\ \eta_z^n(i,j) &= \eta_z\left(\left(i+\frac{1}{2}\right)\Delta x, j\frac{\Delta y}{2}, n\Delta t\right) \end{aligned}\right\} \text{ for odd rows}$$

$$\tag{9}$$

Similar to conventional FDTD, for the present approach magnetic field is computed at $(n+1/2)\Delta t$ and electric field computed at $n\Delta t$ time instances. Since polarization current appears in electric field

update equation, it is computed at $(n+1/2)\Delta t$ time instance. The general form of partial finite difference equations may be represented as follows

$$\left.\frac{\partial}{\partial t} f\right|_{i,j}^{n} = \frac{f|_{i,j}^{n+1/2} - f|_{i,j}^{n-1/2}}{\Delta t} \tag{10}$$

3.1. Material Property Distribution

For material properties distribution, the grid may be seen as superposition of two Yee's grids shifted by half the special step in both the directions. The material properties corresponding to given node may be assigned according to the sub-grid (one of the two overlapping Yee's grids) which it belongs to. Detailed description of material properties distribution in standard FDTD computation domain can be found in [19, 20]. Dielectric and metallic components may be characterized by their permittivity, permeability and conductivity as in the case of standard FDTD. Now to write generalized electromagnetic wave equations for FDTD involving dielectrics, metals as well as plasmas, Eq. (2) may be rewritten as follows

$$\frac{\partial \mathbf{E}}{\partial t} = \frac{1}{\varepsilon_0} \left(\nabla \times \mathbf{H} - \sigma \mathbf{E} - \mathbf{J} \right) \tag{11}$$

For defining plasma in the computation domain electrical conductivity is set to zero and permittivity to permittivity of free space ε_0. $\mathbf{J}$ is plasma polarization current, and it must be zero everywhere except plasma medium. Eq. (6) and Eq. (7) are used to update $\mathbf{J}$ in plasma medium only. Time updating equations based on modified grid may be written very easily in the form of finite difference equation using Eqs. (1), (6), (7), (9)–(11). For results produced in this paper, metal rods are considered perfectly metallic, i.e., electric field inside metal posts is forced to zero. Thus, conductivity profile is not required to be specified, and Eq. (2) can be used instead of Eq. (11). This approach is perfectly valid for obtaining dispersion curves for metal rods of sufficiently high conductivity and rod radius of the order of mm (skin depth for copper at 5 GHz is of the order of 10^{-3} mm hence effect of evanescent waves can be neglected for the studies presented herein ($a = 1$ cm). However, it will be important to consider this effect if one wants to scale the structure for application in lower frequency regime).

3.2. Initialization, Boundary Condition and Post Processing

The computational domain is initialized by hardwiring several sources. As modified grid is superposition of two Yee's grid, sources should be defined at corresponding positions in both the grids. Derivative of Gaussian pulse is used to initialize sources. Bloch periodic boundary condition is used for terminating the computational domain. Implementation of boundary conditions is done to update the terminal nodes in two parts. In the present approach, the main computation domain is spanned by $(2n + 1) \times (2m + 1)$ node points. One row at bottom and one column on the right of node points is defined deliberately for terminating the grid with appropriate boundary condition. Bloch periodic boundary condition is explained in following discussion. One may implement any other boundary condition such as perfectly matched layer (PML), convolution PML etc. as well in a similar manner. The same convention of even and odd rows defined in Eq. (9) is used. For even rows, main computation domain is terminated by η_z, and for odd rows it is terminated by ξ_{xy}. Boundary conditions may be applied as follows

$$\left. \begin{array}{l} \xi_{xy}\left(i, end\right) = \exp(ik_x a) \times \xi_{xy}\left(i, 1\right) \\ \eta_z\left(i, 1\right) = \exp(-ik_x a) \times \eta_z\left(i, end\right) \end{array} \right\} \text{ for even rows}$$

$$\left. \begin{array}{l} \xi_{xy}\left(i, 1\right) = \exp(-ik_x a) \times \xi_{xy}\left(i, end\right) \\ \eta_z\left(i, end\right) = \exp(ik_x a) \times \eta_z\left(i, 1\right) \end{array} \right\} \text{ for odd rows} \tag{12}$$

here k_x is the wave-vector along x-direction; a is the lattice constant; $\xi_{xy}(i, end)$, $\eta_z(i, end)$ denote auxiliary nodes used for implementation of boundary conditions for respective quantities. Boundary conditions should also be applied along y-direction in a similar manner. For triangular lattice, the boundary condition is implemented in two parts. These modified boundary conditions for conventional Yee grid are explained by Umenyi et al. [18]. The same may be implemented in accordance with Eq. (12).

As FDTD simulation evolves over time, fields are recorded at several predefined probe positions. The time domain signal is then converted to frequency domain using fast Fourier Transform (FFT). For efficient use of FFT and sufficient accuracy, FDTD is allowed to evolve for 2^{14} time steps. The peaks in frequency response correspond to frequencies that sustain in the PC, i.e., dispersion curves. Several spurious modes are observed which are purely mathematical and could be easily distinguished in this case from physical modes by looking at the pattern followed by surrounding modes. Physical modes form a smooth curves corresponding to allowed bends. These spurious modes are because of finite frequency resolution while using FFT and truncation of time domain signal to a rectangular window of $N\Delta t$, where N is the number of time steps and Δt the width of a time step [22].

4. RESULTS

4.1. Dispersion Curves of MPC, PMPC and Magnetized PMPC

The dispersion characteristics of 2D MPC and un-magnetized PMPC for $r/a = 0.2$ and normalized plasma frequency $(\omega_p a/2\pi c) = 0.5$ in square and triangular lattice arrangements computed based on standard Yee's grid and modified discretization grid are compared in Fig. 3. Plasma collision frequency is very small and can be neglected for thin plasmas. Only TE polarization is presented as external magnetic field applied in transverse direction does not affect TM polarization. Both results are in excellent agreement confirming the accuracy of the implementation. These results are also in close agreement with non-orthogonal FDTD and modified plane wave expansion method as reported by Qiu and He [23]. Fig. 4 shows dispersion curves of PMPC when placed in external magnetic field of 0.5 *Tesla*. No band gaps are observed in MPC in both square and triangular lattice arrangements for $r/a = 0.2$ up to normalized frequency equal to 4. However, on introducing plasma background photonic bands are up-shifted, and zero order band gaps with normalized cutoff frequencies 0.4797 and 0.4898 respectively for square and triangular lattice are observed. Again when PMPC is subjected to external magnetic field several new bands and band gaps appear. It is seen that the effects of external magnetic field are similar on both square and triangular lattice PMPC. Two flat bands are observed at normalized frequencies 0.4185 and 0.6801 in the case of square lattice and at normalized frequencies 0.4171 and 0.6777 in the case of triangular lattice. Apart from the cutoff band, three higher order band gaps are observed between (0.3139, 0.4883), (0.6801, 0.7585), and (0.8196, 0.8544) for square lattice and (0.3128, 0.5039), (0.6777, 0.7646), and (0.8161, 0.8862) for triangular lattice. The lower flat band lies in photonic band gaps and may be utilized for innovative applications such as tuneable monochromatic filter.
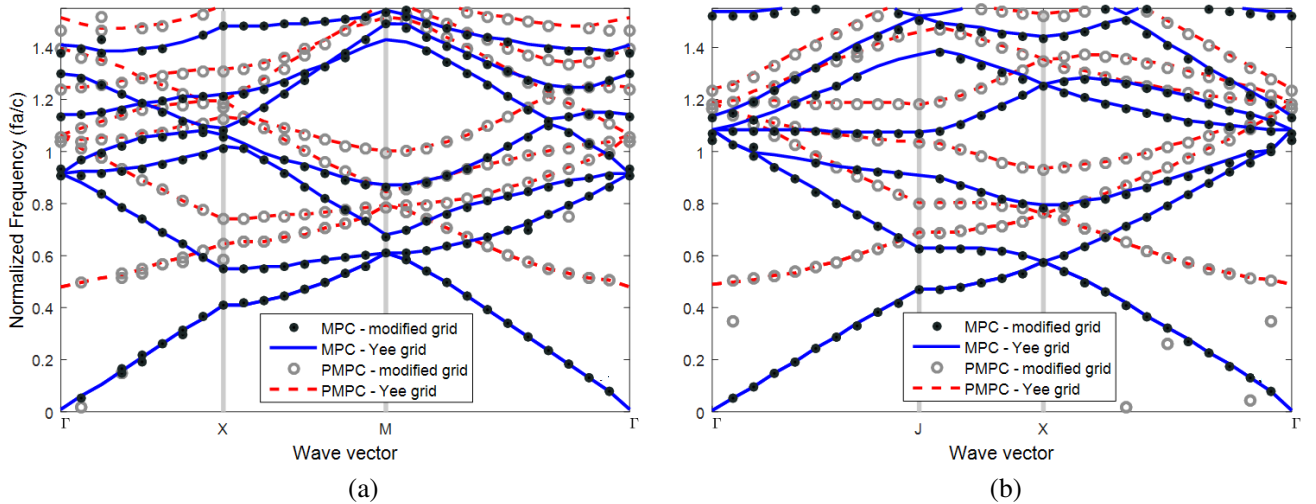
Figure 3. Comparison between dispersion curves obtained based on standard Yee grid and modified grid. Dispersion curves for TE mode of MPC and un-magnetized PMPC in (a) square and (b) triangular lattice arrangements. $r/a = 0.2$ and normalized plasma frequency.
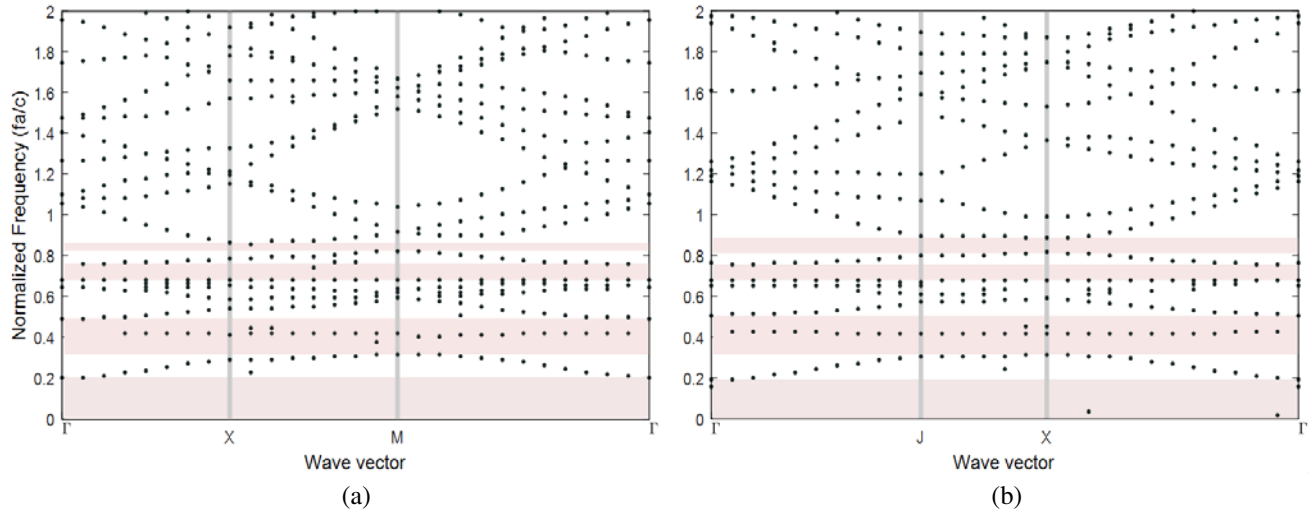
Figure 4. Dispersion curves of magnetized PMPC. Dispersion curves for TE mode of magnetized PMPC in (a) square and (b) triangular lattice arrangements. $r/a = 0.2$, normalized plasma frequency and external magnetic field 0.5 T.
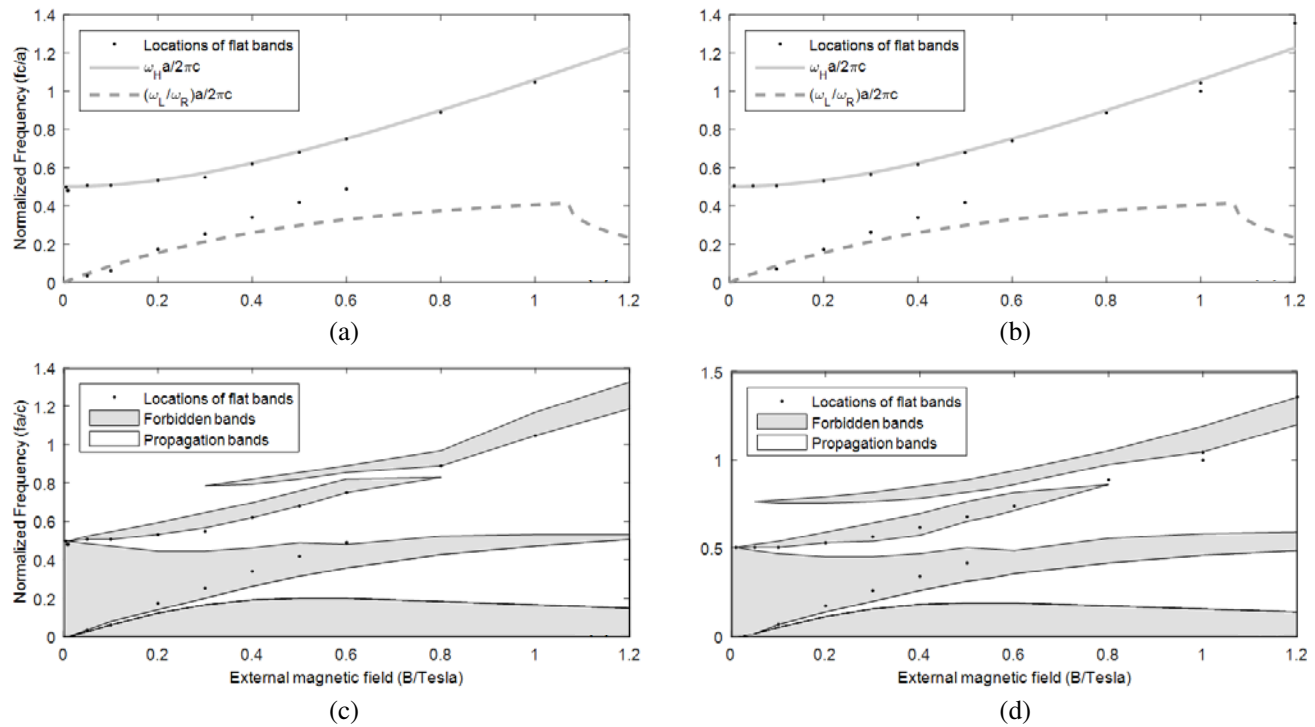
Figure 5. Effect of magnetic field on flat bands and photonic band gaps. Locations of upper flat band for (a) square and (b) triangular lattice arrangement. Variation in photonic band gaps with external magnetic field for (c) square and (d) triangular lattice arrangement.

4.2. Effect of External Magnetic Field on Flat Bands and Photonic Band Gaps

Flat bands appearing in magnetized PMPC are most distinguished feature of its dispersion diagrams. Flat bands indicate dispersion-less propagation. Locations of flat bands and the location and width of photonic band gaps can be tuned dynamically by external magnetic field. Locations of flat bands for

square and triangular lattices are given in Figs. 5(a) and (b) respectively. Locations of upper flat band correspond to upper hybrid frequency $\omega_H = \sqrt{\omega_p^2 + \omega_c^2}$. Thus, it can be concluded that this flat band is caused by cyclotron resonance.

For applied magnetic field less than 0.2 *Tesla*, the lower flat band appears around the real part of ω_L/ω_R. $\omega_L = \frac{1}{2}(-\omega_c + \sqrt{(\omega_c^2 + 4\omega_p^2)})$ and $\omega_R = \frac{1}{2}(\omega_c + \sqrt{(\omega_c^2 - 4\omega_p^2)})$. Figs. 5(c) and (d) shows variation of photonic band gaps with respect to applied magnetic field for square and triangular lattices respectively. Dependence of photonic band gaps and flat bands on magnetic field is similar for both the lattices. It is clear from these figures that with applying external magnetic field new bands appear in the region of cutoff band. The new cutoff frequency first increases with magnetic field and then decreases. The lower frequency of first order band gap is nearly around real part of ω_L/ω_R. The second order band gaps appear because of flattening of first band of un-magnetized PMPC.

5. CONCLUSION

Nonconventional discretization scheme is presented for implementation of FDTD for EM wave propagation in magnetized plasma. FDTD implementation based on the proposed grid is used to study the effect of magnetic field on plasma metallic photonic crystal in square as well as triangular lattice arrangements. This new grid can very easily be extended to three dimensions as well and can be used to solve for any structure involving magnetized plasmas. Some attractive applications involve designing PMPC cavity for gyrotron devices, magnetically controlled plasma waveguides, tuneable monochromatic filter, metamaterials with magnetized plasma inclusions etc. It is observed that the effects of external magnetic field are similar on both square and triangular lattice arrangements. Flat bands appear at the location of upper hybrid frequency up to certain value of magnetic field. When magnetic field is increased beyond 1 Tesla in the case of square lattice arrangement, the flat bands start to show considerable curvatures. Thus, the position of flat bands and photonic band gaps can be tuned dynamically by controlling external magnetic field. The study presented herein based on a new discretization grid will be useful in designing photonic devices involving plasmas in external magnetic field.

ACKNOWLEDGMENT

REFERENCES

1. Yablonovitch, E., "Inhibited spontaneous emission in solid-state physics and electronics," *Phys. Rev. Lett.*, Vol. 58, No. 20, 2059–2062, May 1987.

2. John, S., "Strong localization of photons in certain disordered dielectric superlattices," *Phys. Rev. Lett.*, Vol. 58, No. 23, 2486–2489, Jun. 1987.

3. Sauvan, C., Lalanne, and J.-Hugonin, "Photonics: tuning holes in photonic-crystal nanocavities," *Nature*, Vol. 429, No. 6988, 1–154, 2004.

4. Pan, J., Y. Huo, S. Sandhu, N. Stuhrmann, M. L. Povinelli, J. S. Harris, M. M. Fejer, and S. Fan, "Tuning the coherent interaction in an on-chip photonic-crystal waveguide-resonator system," *Appl. Phys. Lett.*, Vol. 97, No. 10, 101102, 2010.

5. Sun, C., C. H. O. Chen, G. Kurian, L. Wei, J. Miller, A. Agarwal, L. S. Peh, and V. Stojanovic, "DSENT — A tool connecting emerging photonics with electronics for opto-electronic networks-on-chip modeling," *Proceedings of the 2012 6th IEEE/ACM International Symposium on Networks-on-Chip, NoCS 2012*, 201–210, 2012.

6. Inoue, T., M. De Zoysa, T. Asano, and S. Noda, "On-chip integration and high-speed switching of multi-wavelength narrowband thermal emitters," *Appl. Phys. Lett.*, Vol. 108, No. 9, 091101, 2016.

7. Bragheri, F., R. Osellame, and R. Ramponi, "Optofluidics for biophotonic applications," *IEEE Photonics J.*, Vol. 4, No. 2, 596–600, 2012.

8. Sayrin, C., C. Clausen, B. Albrecht, Schneeweiss, and A. Rauschenbeutel, "Storage of fiber-guided light in a nanofiber-trapped ensemble of cold atoms," *Optica*, Vol. 2, No. 4, 353, 2015.

9. Loncar, M., "Molecular sensors: Cavities lead the way," *Nat. Photonics*, Vol. 1, No. 10, 565–567, Feb. 2007.

10. Osorio, D. and A. D. Ham, "Spectral reflectance and directional properties of structural coloration in bird plumage," *J. Exp. Biol.*, Vol. 205, No. 14, 2017–2027, 2002.

11. Vigneron, J. and Simonis, "Natural photonic crystals," *Phys. B Condens. Matter*, Vol. 407, No. 20, 4032–4036, Oct. 2012.

12. Forster, J. D., H. Noh, S. F. Liew, V. Saranathan, C. F. Schreck, L. Yang, J. C. Park, R. O. Prum, S. G. J. Mochrie, C. S. O'Hern, H. Cao, and E. R. Dufresne, "Biomimetic isotropic nanostructures for structural coloration," *Adv. Mater.*, Vol. 22, Nos. 26–27, 2939, Jul. 2010.

13. Fu, T., Z. Yang, Z. Shi, F. Lan, D. Li, and X. Gao, "Dispersion properties of a 2D magnetized plasma metallic photonic crystal," *Phys. Plasmas*, Vol. 20, No. 2, 023109, 2013.

14. Hojo, H. and A. Mase, "Dispersion relation of electromagnetic waves in one-dimensional plasma photonic crystals," *J. Plasma Fusion Res.*, Vol. 80, No. 2, 89–90, 2004.

15. Qi, L., Z. Yang, X. Gao, F. Lan, and Z. Shi, "Transmission characteristics of electromagnetic waves in plasma photonic crystal by a novel FDTD method," *PIERS Proceedings*, 1044–1048, Beijing, China, Mar. 23–27, 2009.

16. Ataei, E., M. Sharifian, and N. Z. Bidoki, "Magnetized plasma photonic crystals band gap," *J. Plasma Phys.*, Vol. 80, No. 04, 581–592, Aug. 2014.

17. Ashutosh, and K. Jain, "FDTD analysis of the dispersion characteristics of the metal pbg structures," *Progress In Electromagnetics Research B*, Vol. 39, 71–88, Feb. 2012.

18. Umenyi, A. V., K. Miura, and O. Hanaizumi, "Modified finite-difference time-domain method for triangular lattice photonic crystals," *J. Light. Technol.*, Vol. 27, No. 22, 4995–5001, Nov. 2009.

19. Schneider, J., "Understanding the finite-difference time-domain method," *Sch. Electr. Eng. Comput.*, 405, 2014.

20. Kunz, K. and R. Luebbers, *The Finite Difference Time Domain Method for Electromagnetics*, Scitech Publishing Inc., Raleigh, 1993.

21. Lewyt, H., "Courant-Friedrichs-Lewy," Mar. 1967.

22. Pereda, J. A., L. A. Vielva, A. Vegas, and A. Prieto, "Computation of resonant frequencies and quality factors of open dielectric resonators by a combination of the finite-difference time-domain (FDTD) and Prony's methods," *IEEE Microw. Guid. Wave Lett.*, Vol. 2, No. 11, 431–433, Nov. 1992.

23. Qiu, M. and S. He, "A nonorthogonal finite-difference time-domain method for computing the band structure of a two-dimensional photonic crystal with dielectric and metallic inclusions," *J. Appl. Phys.*, Vol. 87, No. 12, 8268, 2000.